forum acusticum 2026
8-12 September · Graz, Austria

OPTIMIZING PASSIVE ACOUSTIC FILTERS IN TUBES USING A TRACKING FORMULATION

Felix Huber[1], Fabian Wein[2], Florian Toth[1]

[1] *Institute of Mechanics and Mechatronics, TU Wien, Austria*
[2] *Department of Mathematics, FAU Erlangen-Nürnberg, Germany*

This paper is a revised version of the authors' submitted manuscript that was peer-reviewed by at least two anonymous reviewers.

Abstract

Acoustic topology optimization is a broad topic, with one sub-group being structural optimization. In this discipline, we aim to distribute soundhard material to achieve specific acoustic properties, primarily through a density-based approach. One typical example is the transition zone between two waveguides, soundhard structures that restrict wave propagation and often enforce a unidirectional field.

In this work, we assume that the cross-sections of both waveguides are equal while designing our soundhard structures to achieve a given broadband transmission frequency response. Using lowpass, highpass, bandpass, and bandstop target functions, we synthesize one design for each transmission profile. To avoid modeling thermoviscous losses and ensure manufacturability with standard 3D printing methods, we use a robust filter approach that combines erode, center and dilate filters in a min/max optimization problem. The obtained designs mostly matched the target response within the specified range. The inherent property of structural filters to always transmit low-frequency waves made it hard for the optimizer to converge for highpass and bandpass designs. Lowpass and bandstop filters performed very well, even below the optimization's frequency range. The initial studies showed promising results, motivating future research and parameter studies to further solidify the understanding of the filter devices' working principles.

Keywords: *topology optimization, acoustic tracking, target transmission, robust filter, duct acoustics*

1. Introduction

Since the early days of structural optimization, acoustic topology optimization has played a vital role. While much of the research on acoustic optimization occurs in the field of metamaterials [1], this work focuses on the optimization of macroscale acoustic structures, specifically those operating below the airborne wavelength, by distributing sound-hard material to achieve certain filter characteristics in tubes.

The problem of connecting two waveguides to optimize acoustic transmission properties is not new and has been discussed multiple times. Tang and Lau [2] study the non-uniform transition zone between two tubes with different radii, and Kirby [3] solves a similar problem, using a modified finite element method approach. The first modern topology optimization approach to this problem has been discussed by Wadbro [4] with the aim of impedance matching to achieve broadband transmission, followed by the optimization of devices called acoustic "diodes", which mimic non-reciprocity by mode conversion [5]. Latest applications use this approach for dedicated wave focusing, in so-called sonic black hole (SBH) devices, which exhibit the same slowdown effect as structural acoustic black holes (ABHs) [6].

In this work, we aim to design similar operation devices using density-based topology optimization. In contrast to previous approaches, we do not aim to maximize transmission over varying radii, but rather to achieve a specific frequency response in a waveguide with a constant radius. To achieve this, we introduce a tracking functional that is minimized in a multi-frequency optimization problem, enabling us to optimize passive acoustic filters. This class of devices can be useful for sensor protection, for compensating for unwanted speaker resonances, and, when combined with absorption, as a powerful tool, e.g., for frequency-tuned mufflers.

Mousavi, Berggren, Hägg, *et al.* [7] pointed out that similar devices tend to form thin channels and/or structures, posing a non-physical optimum, which they solved by including viscothermal losses via a special boundary condition [8]. On the contrary, the topologies in this work are obtained by a linear (lossless) modeling approach. To avoid these non-physical optima,

Corresponding author: *felix.huber@tuwien.ac.at.*

we use a min/max formulation, with an erode/dilate robust filter approach [9], to enforce a set of minimum feature and hole sizes.
In Section 2 we provide equations for acoustic modeling, show the necessary equations for the optimization problem, and introduce the tracking functional and its incorporation as constraints in the min/max optimization problem. The target frequency responses and their underlying filter designs, as well as the resulting numerical studies and their optimized designs, are shown and discussed in Section 3. Finally, we summarize the generalized behavior of this class of devices and discuss some future research and applications in Section 5.

2. Acoustic Robust Tracking

We model acoustics in the frequency domain by the Helmholtz equation for inhomogeneous media

$$-\omega^2\kappa^{-1}p - \boldsymbol{\nabla}\cdot\left(\rho_0^{-1}\boldsymbol{\nabla}p\right) = 0 \qquad \text{in } \Omega, \tag{1}$$

with the pressure field p, angular frequency ω and the material parameters bulk modulus κ and density ρ_0. For the optimization problem in this work, sketched in Fig. 2, we want to model input and output tube as infinite waveguides. Therefore, we utilize the Neumann-type excitation

$$\left.\frac{\partial p}{\partial \mathbf{n}}\right|_{\Gamma_{\text{exc}}} = -j\omega\rho_0 v_{\text{n}} \qquad \text{on } \Gamma_{\text{exc}}, \tag{2}$$

with normal velocity v_{n} alongside perfectly matched layers (PMLs) on input and output waveguides. Using the finite element method (FEM) we can discretize Eq. (1) to obtain the algebraic system

$$\underbrace{\left(-\omega^2\mathbf{M} + \mathbf{K}\right)}_{\mathbf{S}}\mathbf{p} = \mathbf{f}, \tag{3}$$

with mass $\mathbf{M}$ and stiffness $\mathbf{K}$ matrices collected in the complex valued system matrix $\mathbf{S}$. The system matrix is assembled from the different regions as

$$\mathbf{S} = \bigwedge_{e=1}^{E}\begin{cases}\mathbf{S}_e & \forall e \in \Omega_{\text{acou}}\\ \widetilde{\mathbf{S}}_e & \forall e \in \Omega_{\text{opt}}\\ \hat{\mathbf{S}}_e & \forall e \in \Omega_{\text{pml}},\end{cases} \tag{4}$$

with the element matricies $\mathbf{S}_e$ for air, $\widetilde{\mathbf{S}}_e$ for material parameterized by our physical pseudo-density variables and $\hat{\mathbf{S}}_e$ for the impedance matched and damped material of the PMLs. The $\bigwedge$ is used as assembly operator for the total number of elements E [10].
To paramterize our material in the optimization domain Ω_{opt} we use a density-based approach. We introduce the element-based physical pseudo-density $\widetilde{\rho}_e$ which is used to inversely scale the material paramters

$$\widetilde{\kappa} = \frac{\kappa}{\widetilde{\rho}_e} \quad \text{and} \quad \widetilde{\rho}_0 = \frac{\rho_0}{\widetilde{\rho}_e}. \tag{5}$$

This scaling results in unchanged material for $\widetilde{\rho}_e = 1$ (solid) and soundhard material for $\widetilde{\rho}_e \approx 0$ (void). Applying this parameterization to the discrete FEM system in Eqs. (3) and (4) yields

$$\widetilde{\mathbf{S}}_e = \widetilde{\rho}_e\mathbf{S}_e, \tag{6}$$

a direct linear scaling of the element matrices in the optimization region.
For the material distribution problem at hand, the design variables are the pseudo-densities ρ_e in the optimization domain. To map them to the physical pseudo-densities used in the FEM model, we apply two kinds of filters. The first one, is a radius based desity filter

$$\bar{\rho}_e = \frac{\sum_{i=1}^{E}\mu(\mathbf{x}_e,\mathbf{x}_i)\rho_i}{\sum_{i=1}^{E}\mu(\mathbf{x}_e,\mathbf{x}_i)}, \tag{7}$$

$$\mu(\mathbf{x}_e,\mathbf{x}_i) = \max(0, R - \|\mathbf{x}_e - \mathbf{x}_i\|), \tag{8}$$

with the element centroid positions $\mathbf{x}_e$ and $\mathbf{x}_i$ and the filter radius R [11]. Second, is a Heaviside-type projection filter, which we use to enforce a binary design.

$$\widetilde{\rho}_e(\bar{\rho}_e;\eta) = \left(\frac{c_{\text{scale}}}{e^{2\beta(\eta-\bar{\rho}_e)}+1}\right) + c_{\text{offset}}, \tag{9}$$

where β defines the steepnes of the function step and the paramter η is used to control the step's center positon. The extrem cases $\eta = 0$ and $\eta = 1$ are refered to as solid-Heaviside and void-Heaviside and are used to control minimum feature or minimum hole size respectively. The constants c_{scale} and c_{offset} are used to map the resulting physical pseudo-densities to the correct bounds. They need to be recomputed for each β/η pair [9], [12].
A typical optimization target is to minimize or maximize the acoustic pressure in a certain region Γ_{out}. This is expressed by

$$\tau_\omega = \mathbf{p}_\omega^{\intercal}\mathbf{L}\mathbf{p}_\omega^{*}, \tag{10}$$

with the diagonal and surface-weighted selection matrix $\mathbf{L}$. To optimize the desgin for a specific frequency response $a(\omega)$, we extend Eq. (10) to the tracking functional

$$g_\omega = \left[\mathbf{p}_\omega^{\intercal}\mathbf{L}\mathbf{p}_\omega^{*} - a(\omega)\right]^2. \tag{11}$$

By normalizing the incident wave, excited by v_{n}, to unity pressure, we can use a normalized frequency response $0 < a < 1$.
To follow the given frequency response as closely as possible, we perform a multi-frequency optimization. The filtering approach used is known as a robust filter [9]. It evaluates three designs (dilated, central, eroded) and optimizes for the worst one. In many cases, e.g., stiffness maximization in elasticity, one can assume that for any design variation within the eroded and dilated design (e.g., during manufacturing), the performance will also be within the evaluated range. This explains the common term robust filter.

For the present time harmonic problem involving resonance effects, we clearly cannot make this claim but merely use the filter approach to concurrently control solid- and void-feature sizes. We do not perform robust optimization in a technical sense but make use of the so-called robust filter, with $\eta_f \in [0.2, 0.5, 0.8]$ for $1 \leq f \leq F$. This results in $K \times F$ physical designs, with K frequencies and $F = 3$ filters. A min/max formulation minimizes a global upper limit α, to which we constrain our tracking functionals. The optimization problem can be written as

$$\min_{\rho} \alpha \tag{12}$$

$$\text{s.t.} \quad \mathbf{S}_{\omega_k}(\widetilde{\rho}(\rho;\eta_f))\mathbf{p}_{\omega_k}(\widetilde{\rho}(\rho;\eta_f)) = \mathbf{f}_{\omega_k}, \tag{13}$$

$$g_{\omega_k}(\mathbf{p}_{\omega_k}(\widetilde{\rho}(\rho;\eta_f))) \leq \alpha, \tag{14}$$

$$1 \leq k \leq K \quad \text{and} \quad 1 \leq f \leq F. \tag{15}$$

To solve this type of problem efficiently, we need to supply the optimizer with the first derivative of our constraints g, with respect to the design variables ρ_e. Indexes for filter and frequency dependence are ommited for clearer writing. We utilize the chainrule to split the derivative in the terms

$$\frac{\partial g}{\partial \rho_e} = \frac{\partial g}{\partial \widetilde{\rho}_e} \sum_{i=1}^{E} \frac{\partial \widetilde{\rho}_e}{\partial \bar{\rho}_i} \frac{\partial \bar{\rho}_i}{\partial \rho_e}. \tag{16}$$

First, we differentiate the tracking functional with respect to the physical pseudo-density, resulting in the partial derivative

$$\frac{\partial g}{\partial \widetilde{\rho}_e} = 4\left[\mathbf{p}^{\mathsf{T}}\mathbf{L}\mathbf{p}^* - a\right]\operatorname{Re}\{\boldsymbol{\lambda}^{\mathsf{T}}\mathbf{S}_e\mathbf{p}\}, \tag{17}$$

with $\boldsymbol{\lambda}$ obtained from the adjoined problem

$$\mathbf{S}^{\mathsf{T}}\boldsymbol{\lambda} = -\mathbf{L}\mathbf{p}^*. \tag{18}$$

The adjoined problem has to be solved for each physical design, resulting in $K \times F$ additional solves for each iteration. The partial derivative of the projection filter is given as

$$\frac{\partial \widetilde{\rho}_e}{\partial \bar{\rho}_i} = \frac{2\beta c_{\text{scale}} e^{2\beta(\eta - \bar{\rho}_i)}}{\left(e^{2\beta(\eta-\bar{\rho}_i)} + 1\right)^2}. \tag{19}$$

Note, that the gradient also changes with different η, requiring a differnt gradient for the different robust settings. The gradient for the radius based density filter is

$$\frac{\partial \bar{\rho}_i}{\partial \rho_e} = \frac{\mu(\mathbf{x}_i, \mathbf{x}_e)}{\sum_{j=1}^{E} \mu(\mathbf{x}_i, \mathbf{x}_j)}. \tag{20}$$

To increase efficiency, the sum in Eqs. (16) and (20) are only evaluated over elements inside the radius R, because they are zero outside anyways.

3. Designing Filters

To test the tracking formulation introduced in Section 2, we synthesized four different filters, similar to the classic filters used in signal processing. A lowpass (LP) filter, a highpass (HP) filter, both with a corner frequency of 2 kHz, and a normalized bandpass (BP) and bandstop (BS) filter, with their center frequencies at 2 kHz and a Q of 4.318.

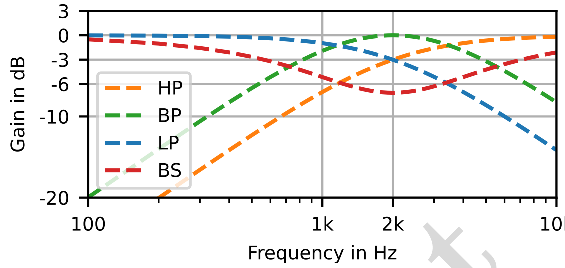

Figure 1: Frequency responses of the target first order filters at 2 kHz. Lowpass (LP), highpass (HP), normalized bandpass (BP) and bandstop (BS) filter with a Q of 4.318. The optimization problem targets tracking these curves.

The design domain used is shown in Fig. 2. We use a circular waveguide with $R_{\text{in}} = 25$ mm and set the maximum device length to $L = 50$ mm. For impedance tube measurements, we can usually assume plane wave propagation up to $f_c = \frac{n}{4}\frac{c_0}{R_{\text{in}}} \approx 3.43$ kHz, for the first mode $n = 1$. However, because we model only the symmetric problem, we expect non-planar wave propagation only after the second mode, which results in $f_c = 6.86$ kHz. For the material modeling, we use standard values for air, the density $\rho_0 = 1.204\,\text{kg}\,\text{m}^{-3}$ and bulk modulus $\kappa = 0.142$ MPa, which are parameterized according to Eq. (5).

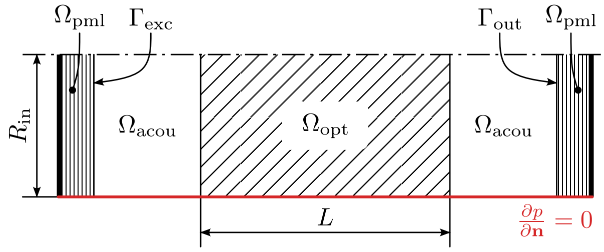

Figure 2: Sketched simulation setup, modeling a radially symmetric waveguide for the material distribution optimization problem in Ω_{opt}. PMLs are used on the input and output tube (Ω_{pml}) alongside Neumann-type excitation on Γ_{exc}. The optimization target is the squared acoustic pressure obtained over Γ_{out}.

We discretized the design using 50 quadratic quadrilateral linear elements in the radial direction, resulting in 100 elements over the length of the design. For the density filter in Eq. (7) a radius of $R = 1.55$ mm was used, which, for full solid/void Heaviside projection, should result in a minimum feature and hole size > 3 mm. The selection of the projection steepness β, introduced in Eq. (9), is mostly a balancing act; a too small value results in a gray design, while a too large value ill conditions the gradient. Therefore, we use "external continuation", starting with $\beta = 1$ and incrementing exponentially within 10 steps to a final value of $\beta = 512$. After a problem for constant β converges, we step β, restart the optimization, and warm-start with the previously obtained design. The optimizer stopped with a Karush-Kuhn-Tucker (KKT) of 1×10^{-6} for most cases; only for the HP design at $\beta \in \{1, 16\}$ did we reach the 500-iteration limit and all except BS terminated early due to numerical dificulties for $\beta = 512$.

The multi-frequency optimization is performed for a set of 12 equally spaced frequencies $\omega_k \in \{2\pi 500\,\text{Hz}, 2\pi 6000\,\text{Hz}\}$, approaching the limit for planar wave propagation. After convergence of the final β-step, the design is thresholded, where elements $\rho_e \leq 0.5$ are considered sound hard, and all others are air. Finally, we evaluate the resulting design from 100 Hz to 10 kHz to also assess our design outside the optimization domain. Due to a normalized incident pressure and constant cross-section of our simulation setup in Fig. 2, Eq. (10) becomes equivalent to the power-scaled transmission coefficient. To evaluate our designs, and compare them to the ideal filters from Fig. 1, we plot the transmission

$$\text{TM} = 10 \log(\tau). \tag{21}$$

3.1. Highpass and bandpass results

One limitation of these structural SBH-filters is their inability to block very low frequencies. The only way to block all low frequencies is to seal the design, which completely prevents wave transmission. Therefore, although our design length is well below the wavelength of the lowest affected frequency, the fixed-length design becomes ineffective at very low frequencies. We use this information to classify our filter designs into two groups; the first, low-cut devices, is discussed here. The designs resulting from the optimization process are shown in Fig. 3, alongside their transmission over frequency according to Eq. (21). Additionally, we plot the respective reference filters from Fig. 1, which were used as optimization target function $a(\omega)$ in the tracking constraints Eq. (11). The lowest point of the target transmission in Fig. 3 is around the lower end of the optimization region (gray), below that, both designs converge to full transmission. As discussed earlier, this is an unavoidable property of structural filters. The low-frequency performance could be extended by allowing longer designs. Looking at the gray optimization region in Fig. 3, we can see that the target transmission is only achieved at specific points, with ripples in between. These optimal points are not correlated with the target frequencies. For the upper optimization range, the actual transmission follows the target quite well; outside the optimization domain, we observe significant deviation, indicating that the design only performs well within the optimized regions' limits. Furthermore, at upper frequencies $f > f_c$, non-planar wave propagation occurs, which

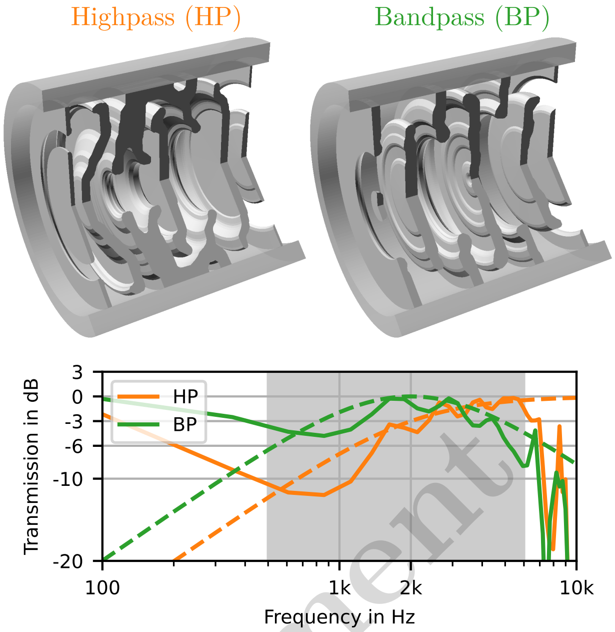

Figure 3: Revolved designs for HP (top-left) and BP filter (top-right), with their transmission coefficient plotted over frequency (bottom). The solid line is the actual transmission coefficient of the thresholded design, while the dashed line indicates the target function. The gray area is the frequency range used in optimization.

also renders the transmission coefficient non-viable. The topologies of both designs look quite similar, with labyrinth-like zig-zag patterns that extend the sound-path and form several resonating chambers. The sizing of the ribs and chambers depends on the target frequency, which tunes the device's impedance to the target transmission. To manufacture these structures, longitudinal ribs could be introduced to support the floating parts. By splitting the design, manufacturing on a normal fused deposition modeling (FDM) printer seems plausible.

3.2. Lowpass and bandstop results

The second class of designs is that which transmits at low frequencies. These are expected to perform much better, as low-frequency transmission is inherent to structural filters. The resulting designs and their transmissions are shown in Fig. 4. Because of the inherent low-frequency transmission, both designs perform very well at the bottom half of the optimization region and below. In the upper half, the BS shows slight target deviations, while the LP shows a hard cut, still within the target range. In the upper frequency region, we observe large deviations, possibly also due to non-planar wave propagation. On the shape of the LP filter, we can clearly derive that a step in diameter, and therefore cross-section, can be used to reflect high frequencies, resulting in a very simple filter design. Although the BS filter seems more complex, we can see the LP-like radius step by comparing the inlet and outlet regions.

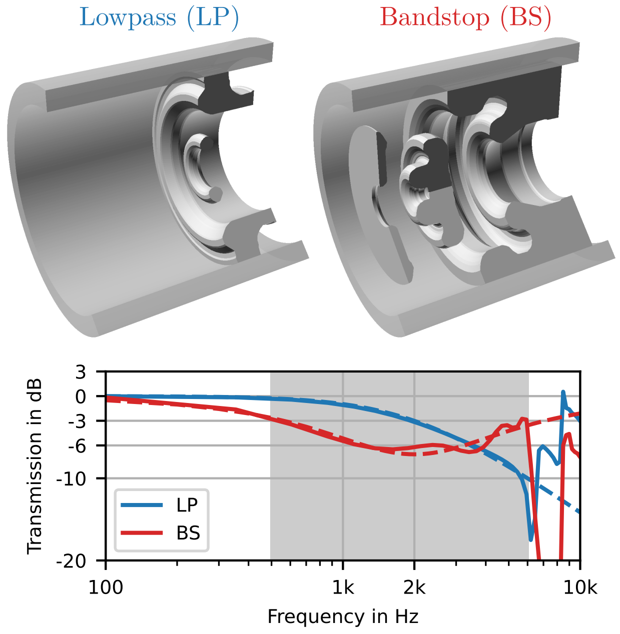

Figure 4: Revolved designs for LP (top-left) and BS filter (top-right), with their transmission coefficient plotted over frequency (bottom). The solid line is the actual transmission coefficient of the thresholded design, while the dashed line indicates the target function. The gray area is the frequency range used in optimization.

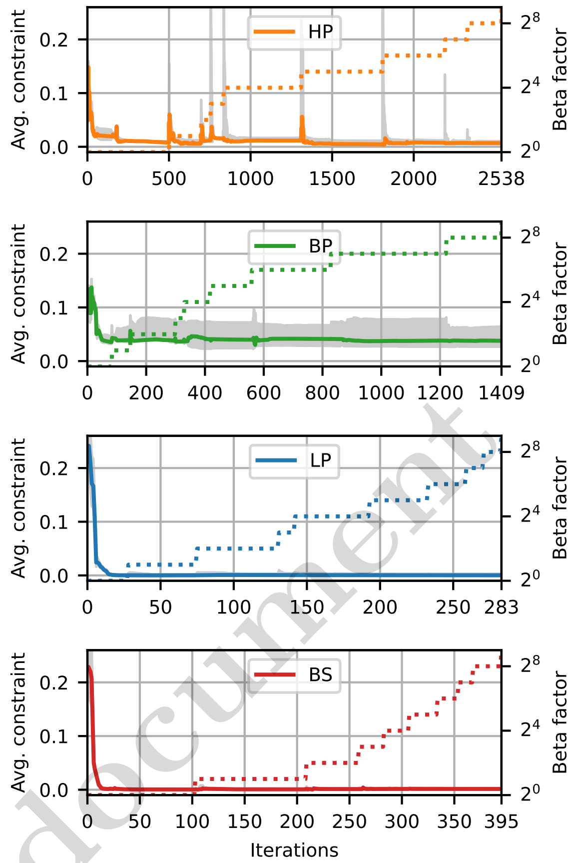

Figure 5: Average constraint value from Eq. (22) over iterations, for the different optimization target filters. The solid line represents the results for a filter parameter $\eta = 0.5$, while the shaded grey area indicates the result range from $\eta = 0.2$ to $\eta = 0.8$. The stepped projection steepness is plotted logarithmically on the right axis.

4. Convergence

The numerical studies conducted in this work were performed using the open-source FEM software openCFS [13] on four logical cores of an Xeon E5-2640 processor. In addition to the highly performant simulation capabilities, openCFS also provides powerful optimization tools. For this work, we implemented the tracking functional from Eq. (11) and tested performance and convergence. To solve the optimization problem at hand, there are several optimizers included in openCFS. However, for wave propagation problems the non-free SNOPT [14] proved to be the most stable.
To evaluate the convergence of the tracking constraints, we introduce the measure

$$g_{\text{avg}}(\eta_f) = \frac{1}{K} \sum_{k=1}^{K} g_{\omega_k}(\eta_f) \tag{22}$$

which is evaluated for each filter parameter η_f. In Fig. 5, we compare the average tracking constraints for $\eta = 0.5$, and indicate the robust filter space of $\eta = 0.2$ to $\eta = 0.8$ as shaded gray area. Furthermore, the stepped projection steppness β is plotted logarithmically with its axis on the right.
Because the tracking constraints are proportional to p^4, all constraints quickly converge to small values. Furthermore, the stepping in β, although necessary to achieve a binary design, does not affect the average destructively. For the low-cut designs (HP and BP), we observe small peaks, especially within the robust filter space (gray). The BP design shows significant differences between the erode and dilate results, indicating that our design is highly sensitive to slight geometric changes. The optimization runs for LP and BP converge quickly and cleanly, showing no significant effect on the β stepping, indicating that external continuation might not be necessary for this type of device.
One clear sign that low-cut devices are significantly harder to optimize is the total number of iterations. The HP filter was the hardest to optimize, requiring over 2500 iterations, followed by the BP filter, which also required well over 1000. The filter designs with low-frequency transmission stayed below 400 total iterations. The respective computation times and memory usage are given in Table 1. Here, we can clearly see that the high number of iterations also translates into increased computation time. Furthermore, the factor between wall and CPU times shows quite good parallelization. Because our FEM problems are small, the memory usage remains manageable below 3 GB across all optimizations.

Table 1: Benchmark results for four logical cores of a Xeon E5-2640 processor.

Design	Wall time	CPU time	Memory
HP	49.49 h	152.35 h	2945 MB
BP	24.00 h	70.46 h	2876 MB
LP	3.65 h	10.61 h	2342 MB
BS	7.13 h	20.63 h	2471 MB

5. Discussion and Outlook

In this article, we present an initial study on the optimization of structural filters in circular tubes. Although we can clearly see that low-cut devices perform significantly worse than low-pass devices, the suggested parameters affecting these properties, filter radius and design length, should be studied in an extensive parameter study. The low-pass devices performed well within their optimization region and even lower frequencies, due to the low-frequency transmission inherent to structural filters. While the obtained designs proved simple and manufacturable, we encountered problems in the higher-frequency optimization region, where evaluations above the tube's cut-on frequency yielded strongly deviating results, especially in the target region. All in all, the study outlines the potential of a structural filter, with many possibilities for further research, particularly in numerical methods parameter selection, manufacturability and measurement.

References

[1] G. Aydın and S. E. San, "Breaking the limits of acoustic science: A review of acoustic metamaterials," en, *Materials Science and Engineering: B*, vol. 305, p. 117 384, Jul. 2024, ISSN: 09215107. DOI: 10.1016/j.mseb.2024.117384.

[2] S. K. Tang and C. K. Lau, "Sound transmission across a smooth nonuniform section in an infinitely long duct," en, *The Journal of the Acoustical Society of America*, vol. 112, no. 6, pp. 2602–2611, Dec. 1, 2002, ISSN: 0001-4966, 1520-8524. DOI: 10.1121/1.1512699.

[3] R. Kirby, "Modeling sound propagation in acoustic waveguides using a hybrid numerical method," en, *The Journal of the Acoustical Society of America*, vol. 124, no. 4, pp. 1930–1940, Oct. 1, 2008, ISSN: 0001-4966, 1520-8524. DOI: 10.1121/1.2967837.

[4] E. Wadbro, "Analysis and design of acoustic transition sections for impedance matching and mode conversion," en, *Structural and Multidisciplinary Optimization*, vol. 50, no. 3, pp. 395–408, Sep. 2014, ISSN: 1615-147X, 1615-1488. DOI: 10.1007/s00158-014-1058-2.

[5] A. H. Bokhari, A. Mousavi, B. Niu, and E. Wadbro, "Topology optimization of an acoustic diode?" en, *Structural and Multidisciplinary Optimization*, vol. 63, no. 6, pp. 2739–2749, Jun. 2021, ISSN: 1615-147X, 1615-1488. DOI: 10.1007/s00158-020-02832-9.

[6] A. Pelat, F. Gautier, S. C. Conlon, and F. Semperlotti, "The acoustic black hole: A review of theory and applications," en, *Journal of Sound and Vibration*, vol. 476, p. 115 316, Jun. 2020, ISSN: 0022460X. DOI: 10.1016/j.jsv.2020.115316.

[7] A. Mousavi, M. Berggren, L. Hägg, and E. Wadbro, "Topology optimization of a waveguide acoustic black hole for enhanced wave focusing," en, *The Journal of the Acoustical Society of America*, vol. 155, no. 1, pp. 742–756, Jan. 1, 2024, ISSN: 0001-4966. DOI: 10.1121/10.0024470.

[8] A. Mousavi, M. Berggren, and E. Wadbro, "Extending material distribution topology optimization to boundary-effect-dominated problems with applications in viscothermal acoustics," en, *Materials & Design*, vol. 234, p. 112 302, Oct. 2023, ISSN: 02641275. DOI: 10.1016/j.matdes.2023.112302.

[9] F. Wang, B. S. Lazarov, and O. Sigmund, "On projection methods, convergence and robust formulations in topology optimization," en, *Structural and Multidisciplinary Optimization*, vol. 43, no. 6, pp. 767–784, Jun. 2011, ISSN: 1615-147X, 1615-1488. DOI: 10.1007/s00158-010-0602-y.

[10] M. Kaltenbacher, *Numerical Simulation of Mechatronic Sensors and Actuators*, en. Berlin, Heidelberg: Springer Berlin Heidelberg, 2007, ISBN: 978-3-540-71359-3. DOI: 10.1007/978-3-540-71360-9.

[11] T. E. Bruns and D. A. Tortorelli, "Topology optimization of non-linear elastic structures and compliant mechanisms," en, *Computer Methods in Applied Mechanics and Engineering*, vol. 190, no. 26–27, pp. 3443–3459, Mar. 2001, ISSN: 00457825. DOI: 10.1016/S0045-7825(00)00278-4.

[12] J. K. Guest, J. H. Prévost, and T. Belytschko, "Achieving minimum length scale in topology optimization using nodal design variables and projection functions," en, *International Journal for Numerical Methods in Engineering*, vol. 61, no. 2, pp. 238–254, Sep. 14, 2004, ISSN: 0029-5981, 1097-0207. DOI: 10.1002/nme.1064.

[13] openCFS, *Coupled Field Simulation*, https://gitlab.com/openCFS/cfs, 2025.

[14] P. E. Gill, W. Murray, and M. A. Saunders, "SNOPT: An SQP Algorithm for Large-Scale Constrained Optimization," en, *SIAM Review*, vol. 47, no. 1, pp. 99–131, Jan. 2005, ISSN: 0036-1445, 1095-7200. DOI: 10.1137/S0036144504446096.